Thin-film morphology and transistor performance of alkyl-substituted triethylsilylethynyl anthradithiophenes†

John E. Anthony,*[a] Sankar Subramanian,[a] Sean R. Parkin,[a] Sung Kyu Park[b] and Thomas N. Jackson[b]

Studies of soluble small-molecule semiconductors based on pentacene and anthradithiophene chromophores have generally shown that molecules with strong two-dimensional solid-state interactions yield high-performance thin-film transistors, while similar compounds with one-dimensional solid-state interactions form thin-film devices with significantly worse performance. As a further exploration of this issue, we describe here the synthesis and device characterization of soluble anthradithiophene derivatives functionalized at the periphery of the chromophore with small (C_1–C_3) alkyl chains that subtly alter the solid-state arrangements of the molecules. We demonstrate that these changes in crystal packing have significant impact on both thin-film formation and field-effect mobility. In general, materials with even nominal two-dimensional close contacts between molecules tended also to exhibit two-dimensional film growth, and generally better device performance than those with strictly one-dimensional interactions.

1. Introduction

A significant driving force in the development of new organic semiconductors has been the potential for low-cost solution-based fabrication techniques such as spin-coating[1] and ink-jet printing,[2] allowing device fabrication on large area flexible substrates.[3] In our studies of substituted pentacenes[4] and anthradithiophenes[5] (ADTs) for use in the solution-fabrication of organic field-effect transistors (OFETs), we observed that materials that adopt a one-dimensional (1-D) π-stacking arrangement (where there is only one stacking neighbor above the aromatic plane, and one below—Fig. 1(a)) exhibited several orders of magnitude worse OFET performance than materials with two-dimensional (2-D) π-stacking arrangements (where each aromatic molecule has two close-contact neighbors above the aromatic plane, and two below—Fig. 1(c)). Band-structure calculations for π-stacked pentacenes showed large bandwidths in both 1-D and 2-D stacked materials,[6] and single-crystal studies of compounds adopting both stacking motifs showed the difference in hole mobility was only a factor of ~2.[7] The difference in thin-film devices likely arises from changes in thin-film morphology, which has long been cited as a critical parameter for device performance in solution-cast materials.[8–10] Close inspection of 2-D π-stacked materials shows that this arrangement is in fact an interdigitation of 1-D π-stacked molecules—thus there must be a continuum, from strictly isolated 1-D stacks, through strongly interacting 1-D stacks, to 2-D stacked materials. Because we use crystallographic analysis for rapid screening of potential OFET materials, we desired to determine the point in this continuum where the properties of the material change from "1-D" performance to "2-D" performance. We have shown that changes in trialkylsilyl substituents in these compounds lead to significant changes in crystal packing, and similar effects have been observed in acene monothiophenes.[10] We describe here the more subtle effect of thiophene alkylation on the crystal packing of soluble anthradithiophenes, and describe the effects of these changes on film formation and device performance.

2. Experimental

2.1 Synthetic details

General. Solvents were purchased from Fisher, tetrahydrofuran was distilled over sodium–benzophenone under N_2, and triethylsilyl acetylene was purchased from GFS Chemicals. NMR spectra were measured on Varian (Gemini 200 MHz/Unity 400 MHz) spectrometers, with chemical shifts reported in ppm relative to $CDCl_3$ as internal standard. UV–vis spectra were
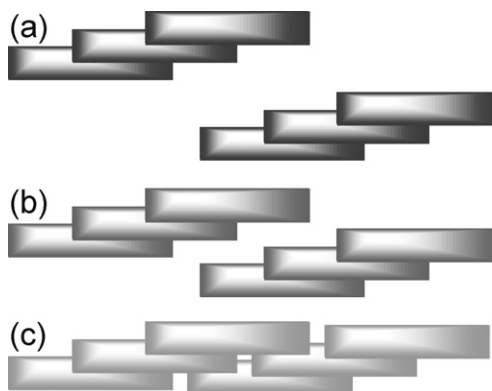
[a]Department of Chemistry, University of Kentucky, Lexington, KY, 40506, USA. E-mail: anthony@uky.edu
[b]Department of Electrical Engineering, Penn State University, University Park, PA, 16802, USA. E-mail: tnj1@psu.edu

Fig. 1 The transition in π-stacking arrangements from isolated 1-D π-stacks (a), through interacting 1-D π-stacks (b), to 2-D π-stacks (c).

measured on a Shimadzu UV-2501PC. Mass spectrometry was performed in EI mode at 70 eV or MALDI with TCNQ matrix on a JEOL (JMS-700T) mass spectrometer. Cyclic voltammetry was carried out on a BAS CV-50W at a scan rate of 150 mV s^{-1}, with a Pt disc as working electrode, Ag/AgCl as reference and Pt auxiliary electrode. Bu_4NPF_6 (0.1 M) was used as electrolyte and ferrocene as an internal standard. Combustion analysis was performed by Desert Analytics, Tucson, AZ. Melting points were measured by differential scanning calorimetry.

General procedure for the preparation of 5-alkyl thiophene-2,3-dicarboxaldehydes[11]. To a flame dried flask containing thiophene-2,3-diacetal (21 mmol) dissolved in 60 mL THF was slowly added n-BuLi (27.4 mmol) at −78 °C. After 1 h, alkyl iodide (29.5 mmol) was added, the reaction mixture was allowed to warm to room temperature, and was stirred overnight. The reaction mixture was quenched with water, extracted with ether, and the ether evaporated. Without purification, the diacetal was hydrolyzed by stirring in 3 M HCl–THF (1 : 1) for 1 h. The resulting product was extracted and purified by column chromatography using hexanes–dichloromethane eluent (2 : 3).

5-Methyl thiophene-2,3-dialdehyde (3). Yield = 62%. ^{1}H NMR (200 MHz): δ 2.55 (s, 3H), 7.27 (s, 1H), 10.27 (s, 1H), 10.34 (s, 1H) ppm. ^{13}C NMR (50 MHz): δ 16.16, 128.31, 144.29, 145.55, 150.42, 182.38, 184.91 ppm. MS (EI, 70 eV) m/z 154 (M$^+$), 125 (M$^+$ − CHO).

5-Ethyl thiophene-2,3-dialdehyde (4). Yield = 79%. ^{1}H NMR (200 MHz): δ 1.37 (t, J = 7.5 Hz, 3H), 2.92 (q, J = 7.6 Hz, 2H), 7.34 (s, 1H), 10.33 (s, 1H), 10.39 (s, 1H) ppm. ^{13}C NMR (50 MHz): δ 14.99, 23.71, 126.24, 143.98, 144.80, 157.59, 182.20, 184.85 ppm. MS (EI, 70 eV) m/z 168 (M$^+$), 140 (M$^+$ − CHO).

5-Propyl thiophene-2,3-dialdehyde (5). Yield = 66%. ^{1}H NMR (200 MHz): δ 0.94 (t, J = 7.3 Hz, 3H), 1.68 (m, 2H), 2.80 (t, J = 7.6 Hz, 2H), 7.27 (s, 1H), 10.26 (s, 1H), 10.32 (s, 1H) ppm. ^{13}C NMR (50 MHz): δ 13.51, 24.41, 32.43, 127.07, 143.96, 145.04, 156.03, 182.31, 184.97 ppm. MS (EI, 70 eV) m/z 182 (M$^+$), 154 (M$^+$ − CHO).

General procedure for the preparation of substituted ADT quinones. A few drops of 15% aqueous KOH solution were added to a mixture of 1,4-cyclohexanedione (0.6 g, 5.5 mmol) and 5-alkyl thiophene dialdehyde (11.0 mmol) dissolved in tetrahydrofuran–ethanol (5 : 15 mL), and the resulting suspension stirred at room temperature for 3 h. The yellow precipitate was filtered through a Büchner funnel, washed with ether and dried in air to yield the desired product, which was used as produced.

2,8-Dimethyl anthradithiophene-5,11-dione (6). Yield = 70%. MS (MALDI) m/z 348 (100%, M$^+$).

2,8-Diethyl anthradithiophene-5,11-dione (7). Yield = 65%. MS (MALDI) m/z 377 (100%, M$^+$ + 1).

2,8-Dipropyl anthradithiophene-5,11-dione (8). Yield = 65%. MS (MALDI) m/z 404 (100%, M$^+$).

General procedure for the synthesis of triethylsilylethynyl ADTs. n-BuLi (1.86 mL, 4.66 mmol) was added to triethylsilyl acetylene (5.32 mmol) in hexanes (50 mL) under dry N_2 at room temperature in a dry 500 mL flask, and the resulting solution was stirred for 30 min. The alkyl-substituted ADT quinone (1.33 mmol) was then added, followed by additional hexanes (200 mL), and the resulting suspension stirred at 66 °C until the quinone had completely dissolved (∼12 h). $SnCl_2$ (0.9 g, 3.99 mmol), 0.5 mL of water and 1.5 mL of 10% H_2SO_4 were then added to the reaction mixture, which was maintained at 66 °C for an additional 5 h. The reaction mixture was cooled and dried over anhydrous $MgSO_4$. It was then purified by filtration through a silica-gel filled fritted funnel, eluting with hexanes. The solvent was evaporated and the products crystallized from hexanes.

2,8-Dimethyl-5,11-bis(triethylsilylethynyl)ADT (9). Yield = 51%. ^{1}H NMR (200 MHz): δ 0.91 (q, J = 7.6 Hz, 12H), 1.25 (t, J = 7.8 Hz, 18H), 2.65 (s, 6H), 7.09 (s, 2H), 8.89 (s, 2H), 9.00 (s, 2H) ppm. ^{13}C NMR (50 MHz): δ 4.94, 8.04, 17.15, 103.71, 103.83, 103.95, 106.20, 106.41, 106.63, 116.23, 117.23, 118.23, 119.35, 119.43, 119.61, 119.71, 121.35, 123.95, 129.56, 129.59, 129.84, 130.09, 130.12, 140.44, 140.48, 141.28, 141.30, 144.55, 144.59. MS (EI, 70 eV) m/z 594 (100%, M$^+$), 595 (50%, M$^+$ + 1). Anal. calcd % C: 72.66, % H: 7.11; found % C: 72.38, % H: 6.98; mp: 276 °C.

2,8-Diethyl-5,11-bis(triethylsilylethynyl)ADT (10). Yield = 61%. ^{1}H NMR (200 MHz): δ 0.92 (q, J = 7.8 Hz, 12H), 1.26 (t, J = 7.7 Hz, 18H), 1.46 (t, J = 7.5 Hz, 6H), 3.00 (q, J = 7.46 Hz, 4H), 7.12 (s, 2H), 8.92 (s, 2H), 9.03 (s, 2H) ppm. ^{13}C NMR (50 MHz): δ 4.91, 7.91, 14.90, 24.94, 103.96, 106.18, 117.26, 119.39, 119.53, 119.62, 119.86, 119.95, 129.70, 130.19, 140.05, 141.22, 151.84, 151.89 ppm. MS (EI, 70 eV) m/z 622 (25%, M$^+$), 623 (15%, M$^+$ + 1). Anal. calcd % C: 73.25, % H: 7.44; found % C: 73.21, % H: 7.51; mp: 215 °C.

2,8-Dipropyl-5,11-bis(triethylsilylethynyl)ADT (11). Yield = 56%. ^{1}H NMR (400 MHz): δ 0.92 (q, J = 8.0 Hz, 12H), 1.07 (t, J = 7.4 Hz, 6H), 1.25 (m, 18H), 1.86 (m, 4H), 2.94 (t, J = 7.2 Hz, 4H), 7.12 (s, 2H), 8.91 (s, 2H), 9.02 (s, 2H) ppm. ^{13}C NMR (100 MHz): δ 4.95, 8.04, 13.97, 23.98, 33.70, 103.86, 103.96, 106.35, 117.18, 119.49, 119.57, 119.76, 119.85, 120.28, 129.59, 130.08, 130.10, 140.04, 140.08, 141.11, 150.15, 150.19. MS (EI, 70 eV) m/z 650 (100%, M$^+$), 651 (50%, M$^+$ + 1). Anal. calcd % C: 73.78, % H: 7.73; found % C: 73.55, % H: 7.76; mp: 225 °C.

2.2 Crystallography

X-Ray crystallographic studies were performed on a Nonius KappaCCD diffractometer, with graphite monochromated MoKα radiation. Data were integrated, scaled, merged and corrected for Lorentz-polarization effects using the HKL-SMN package.[12] The structures were solved by direct methods using SHELXS97[13] and refined using SHELXL97.[13] Hydrogen atoms were found in difference maps but subsequently placed at calculated positions and refined using a riding model. Non-hydrogen atoms were refined with anisotropic displacement parameters. In common with other anthradithiophenes, the

This journal is © The Royal Society of Chemistry 2009

J. Mater. Chem., 2009, **19**, 7984–7989 | 7985
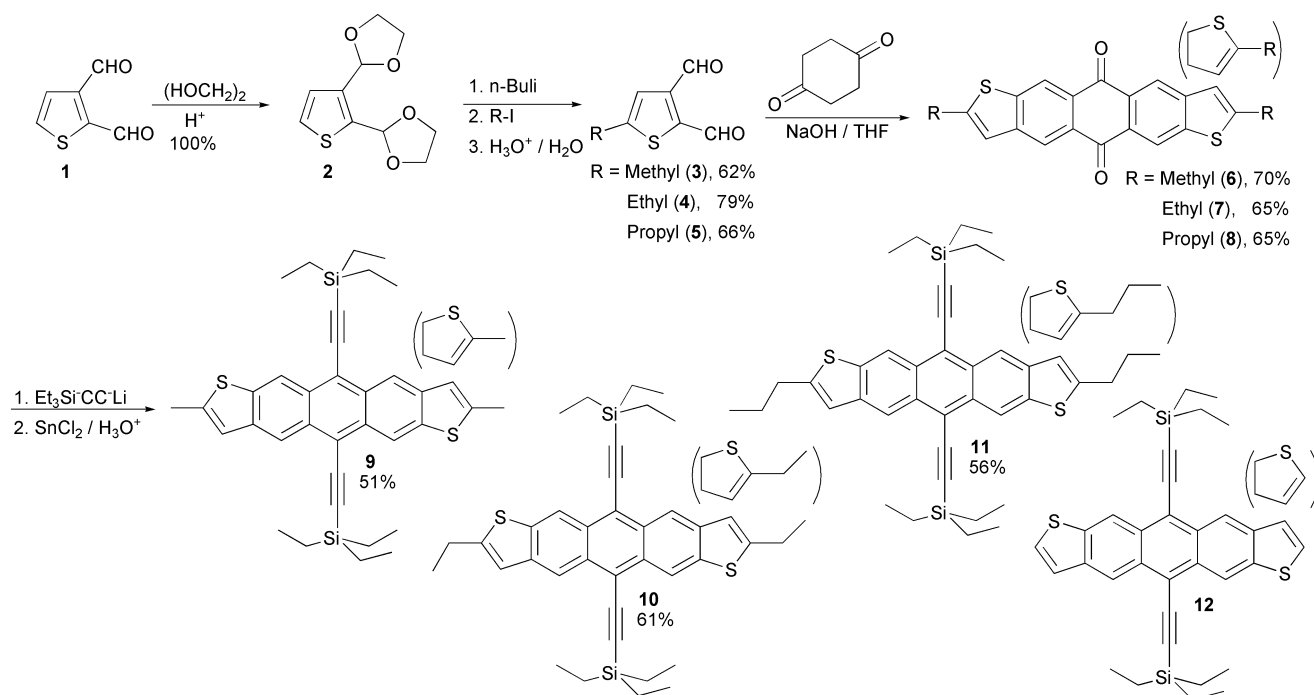
Scheme 1 Synthesis of alkyl ADT derivatives **9–11** and parent compound **12**

R = Methyl (**3**), 62%
Ethyl (**4**), 79%
Propyl (**5**), 66%

R = Methyl (**6**), 70%
Ethyl (**7**), 65%
Propyl (**8**), 65%

thiophene rings were disordered by a 180° flip. Structural data for **12** were reported previously.[5]

Crystal data for compound 9. $C_{36}H_{42}S_2Si_2$, $M = 595.00$, triclinic, $a = 7.14$, $b = 10.32$, $c = 11.24$ Å, $\alpha = 83.81°$, $\beta = 89.24°$, $\gamma = 81.28°$, $V = 814.2$ Å^3, $T = 90.0(2)$ K, space group $P\bar{1}$, $Z = 1$, 7355 reflections measured, 3710 unique ($R_{int} = 0.0557$), $R_1[I > 2\sigma(I)] = 0.0508$.

Crystal data for compound 10. $C_{38}H_{46}S_2Si_2$, $M = 623.05$, triclinic, $a = 7.90$, $b = 10.49$, $c = 10.84$ Å, $\alpha = 76.32°$, $\beta = 88.44°$, $\gamma = 88.96°$, $V = 872.64$ Å^3, $T = 150(1)$ K, space group $P\bar{1}$, $Z = 1$, 7521 reflections measured, 3710 unique ($R_{int} = 0.0251$), $R_1[I > 2\sigma(I)] = 0.0542$.

Crystal data for compound 11. $C_{40}H_{50}S_2Si_2$, $M = 651.10$, triclinic, $a = 7.41$, $b = 11.23$, $c = 12.00$ Å, $\alpha = 73.61°$, $\beta = 76.79°$, $\gamma = 74.42°$, $V = 911.11$ Å^3, $T = 90.0(2)$ K, space group $P\bar{1}$, $Z = 1$, 8230 reflections measured, 4154 unique ($R_{int} = 0.0299$), $R_1[I > 2\sigma(I)] = 0.0497$.

2.3 OFET device fabrication

Bottom-contact thin-film transistors were constructed on a heavily doped silicon wafer that also served as gate electrode. The thermally grown oxide layer 200–370 nm thick was used as dielectric. Gold source and drain electrodes were deposited on the device by thermal evaporation, with channel widths of 120–220 μm and channel lengths of 5–20 μm. Solutions of functionalized ADTs (2 wt% in toluene) were drop cast on the device surface and the solvent allowed to evaporate in air.

3. Results and discussion

Typically, unsubstituted acenes adopt an edge-to-face solid-state arrangement with strong two-dimensional electronic coupling.[14] Functionalization of acenes (or heteroacenes such as ADT) with trialkylsilylethynyl groups at the *peri*-positions of the aromatic backbone causes these chromophores to adopt a variety of π-stacked arrangements that can be altered by changing the size of the alkyne substituent.[15,16] For functionalized pentacenes, we typically observed more than three orders of magnitude difference in thin-film performance between 2-D π-stacked materials and 1-D π-stacked materials, which we attributed to differences in electronic coupling. However, recent single-crystal studies comparing the mobility of 2-D and 1-D π-stacked pentacenes
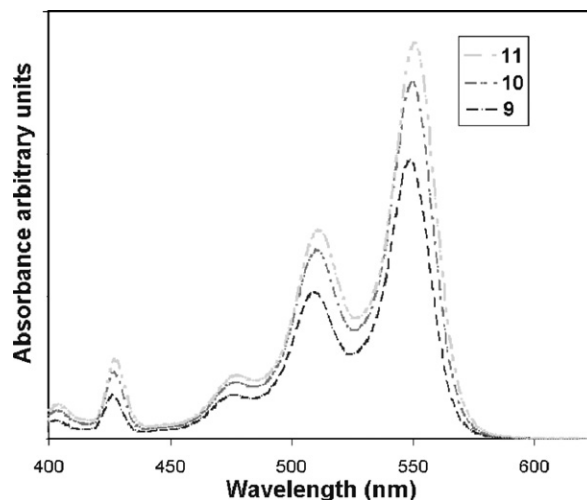
Fig. 2 UV–visible spectra of ADT derivatives in dichloromethane.

suggested a difference of only a factor of 2 in mobility between these two systems.[7] Similar issues are observed in other organic systems—for example, two-dimensional interactions in pentacene
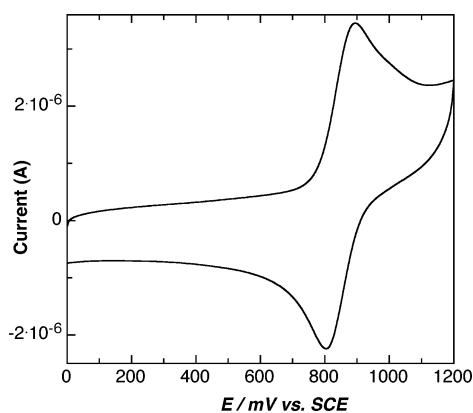

Fig. 3 Cyclic voltammetric trace of representative ADT **11**.

lead to relatively high single-crystal mobility as well as uniform thin films and excellent device performance.[17] In contrast rubrene, with strong one-dimensional interactions and extraordinary single-crystal hole mobility[18] exhibits poor thin-film morphology and thus significantly worse thin-film mobility.[19] Along with crystal packing, the poor film morphology of rubrene may also arise from twisting of the rubrene backbone when deposited on oxide surfaces.[20] Research on columnar discotic liquid crystals also showed strong dependence between functionalization and thin-film growth.[21] These results encouraged us to probe the influence of crystal packing on film morphology in the easily modified ADT series of materials. Alkyl-substituted ADTs **9–11** are easily prepared as shown in Scheme 1, using variations of previously reported methods.[11,22] As with all previously reported ADTs,[11,22–24] these quinones and their subsequent alkyne-functionalized derivatives are synthesized as an inseparable mixture of *syn*- and *anti*-isomers. The UV-vis absorption spectra of alkyl-substituted functionalized ADTs **9–11** recorded in dichloromethane show the lowest energy absorption at 550 nm (Fig. 2),
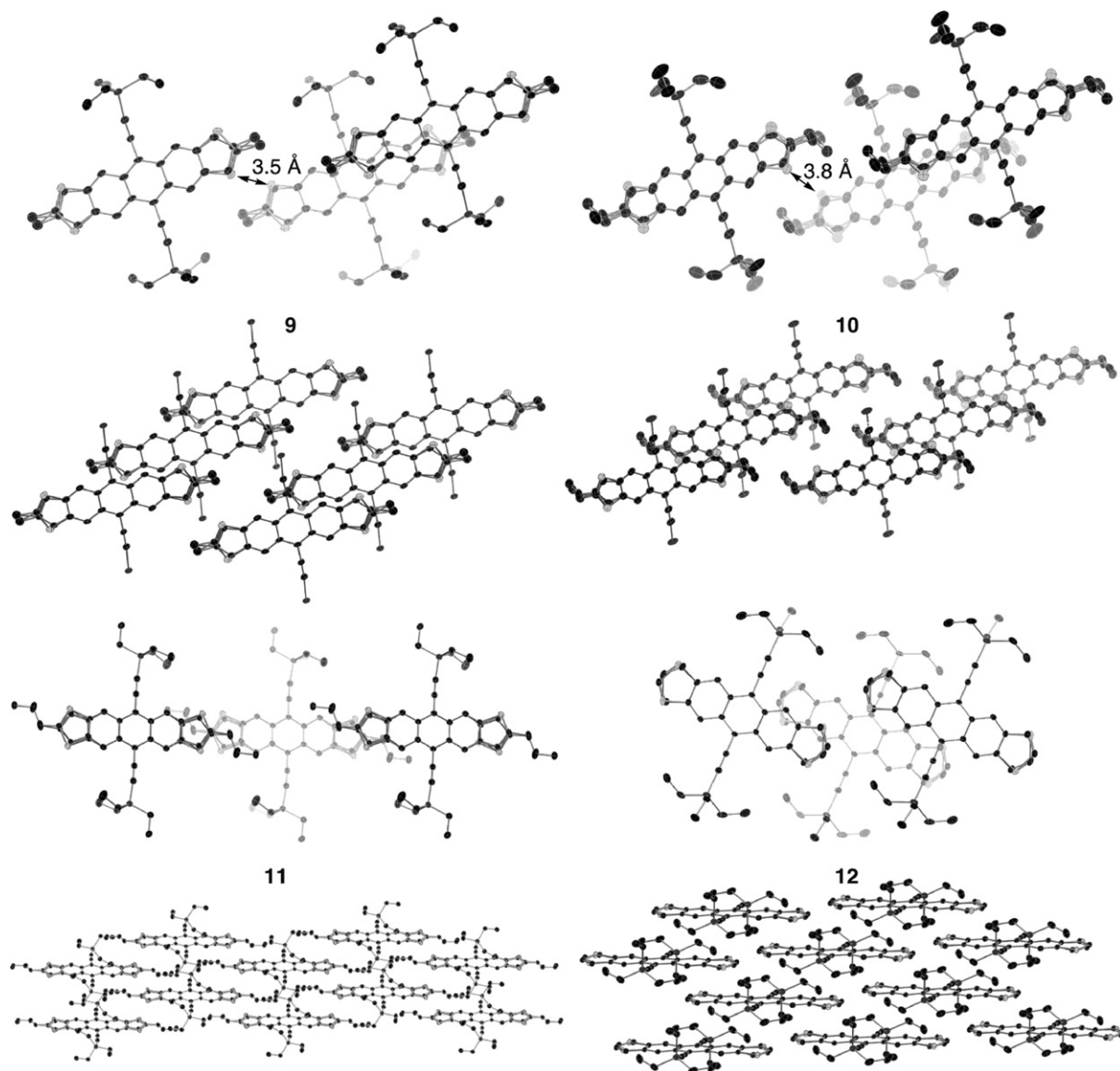

Fig. 4 Crystal packing arrangements for **9–12**. Some silane alkyl groups are omitted for clarity.

This journal is © The Royal Society of Chemistry 2009

J. Mater. Chem., 2009, **19**, 7984–7989 | 7987

which matches well with that of **12** (560 nm).[23] From electrochemical studies (a representative trace for **11** is shown in Fig. 3), the oxidation potential of the derivatives **9–11** was 0.84 V *vs.* SCE, a slight decrease from the 0.90 V *vs.* SCE reported for **12**. These results demonstrate that the electronic properties of the molecules remain similar—the differences in device performance arise from changes associated with differences in crystal packing.

High-quality single crystals of ADTs **9–11** were easily grown from hexanes, and their solid-state arrangements determined by single-crystal X-ray diffraction. Fig. 4 shows the semiconductor molecules (light-shaded molecule) along with their two closest neighbors in the plane above the molecule (dark-shaded molecules), as well as a depiction of the bulk packing motif for each derivative. Both the methyl and the ethyl derivatives **9** and **10** exhibit predominant 1-D π-stacking,[15] although with different spacing between adjacent stacks. A few atoms within the stacks of methyl derivative **9** are separated by as little as 3.5 Å, potentially allowing inter-stack electronic coupling.[25] Peripheral carbon atoms in the one-dimensional stacks of ethyl derivative **10** are separated by at least 3.8 Å, which lies outside the van der Waals radii for adjacent carbon atoms, leading to poor electronic coupling between the adjacent stacks. Propyl-substituted ADT **11** adopts a two-dimensional π-stacking motif similar to that seen in the parent triethylsilylethynyl ADT **12**. However, the arrangement of the propyl substituents leads to a significant increase in interplanar spacing in stacks of **11**, yielding a closest intermolecular contact of 3.8 Å. This large interplanar spacing significantly diminishes electronic coupling between the aromatic molecules, curtailing hole transport even though the two-dimensional π-stacking motif typically yields high-performance transistors.[25] The crystal packings of these four molecules comprise an interesting cross-section of solid-state arrangements: a weakly interacting 2-D π-stacked motif (**11**), a strongly interacting 2-D π-stacked motif (**12**), a transitional motif with strongly interacting 1-D π-stacks (**9**), and isolated 1-D π-stacks (**10**).

Several studies of the thin-film morphology of **12** have already been reported.[26–28] This benchmark semiconductor dewets from most common transistor substrates (even monolayer-treated ones), and requires deposition by doctor-blade, or spin-coating followed by solvent vapor annealing, to yield uniform films with large plate-like crystalline domains that substantially cover the device substrate. Alkyl derivatives **9–11** experienced no such dewetting issues, and films were easily formed on substrates by drop-casting from a 2 wt% solution of the semiconductor in toluene, followed by slow evaporation of the solvent in air. The morphology of the resulting films was studied by optical microscopy (Fig. 5), revealing dramatic differences between the materials. Both of the materials with 2-D π-stacked crystal packing (**9** and **11**) yielded films with pronounced two-dimensional film growth over the substrate (Fig. 5). Methyl derivative **9**, possessing strong 1-D π-stacking interactions coupled with weak inter-stack interactions, formed large grains that easily spanned the active channel of bottom-contact device substrates. Propyl derivative **11** also yielded essentially 2-D film growth, although the weak interactions in this crystal led to very small grains, with poor continuity in the film grown over the device substrate. In contrast to **9** and **11**, derivative **10** did not grow two-dimensional films; in keeping with the strong 1-D interactions in the crystal, this derivative formed long needles that grew off the substrate surface, yielding poor surface coverage and poor connectivity between grains. Although this type of film growth has proven beneficial for stacked devices such as photovoltaics,[29] it is clearly inappropriate for planar devices such as OFETs.

Typical transfer curves for the TFT characteristics of the functionalized ADTs are shown in Fig. 5. Thin-film hole mobility and threshold voltages were extracted from the linear region of the gate voltage *versus* square root of drain current curve. Devices fabricated from methyl derivative **9** exhibited hole mobility roughly equal to those formed from non-alkylated **12**,[5,30] with extracted hole mobility in the range of 0.1 to 0.4 cm^2 V^{-1} s^{-1} and on–off current ratio of 10^5. These mobility values indicate that this transitional crystal packing retains sufficient two-dimensional interaction to yield film morphology and electronic coupling adequate for OFET applications. Mobilities for devices made
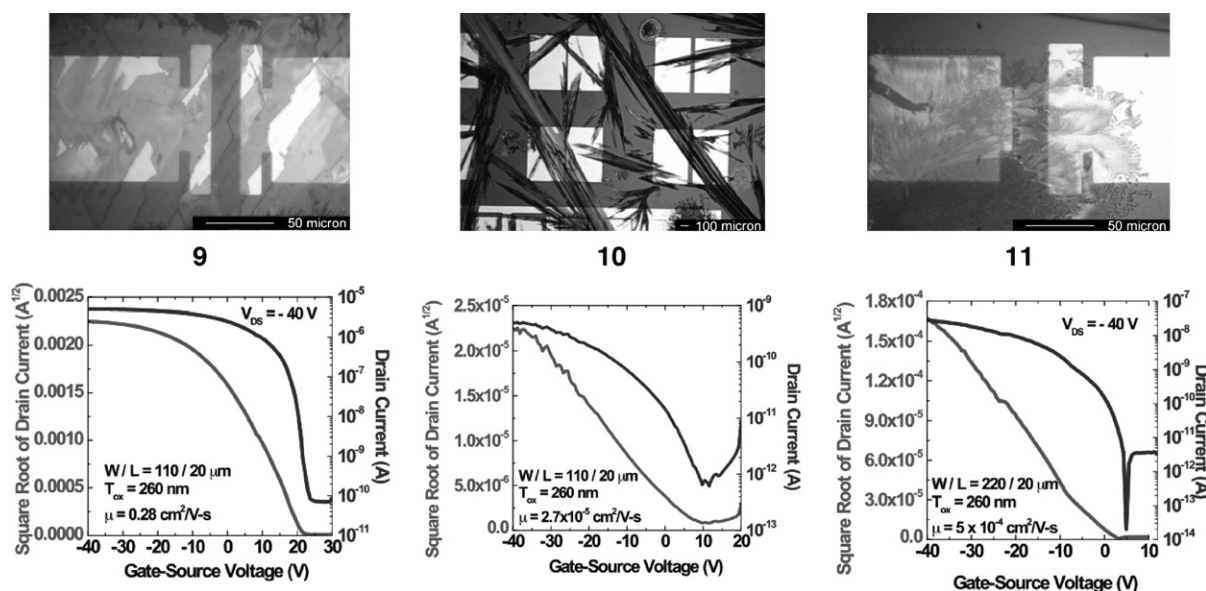

Fig. 5 Film morphology and transistor performance of **9–11**.

with **10** and **11** were significantly lower. For **11**, which exhibits the desired two-dimensional film growth but possesses large interplanar spacing in the crystal, hole mobility ranged from 10^{-3} to 10^{-4} cm^2 V^{-1} s^{-1}. Mobility for the 1-D π-stacked **10** was typically an order of magnitude worse (<10^{-5}cm^2 V^{-1} s^{-1}), due to the poor morphology of the solution-deposited films combined with the unidirectional electronic coupling imposed by the one-dimensional π-stacking interactions. The difference in performance of the devices made from **9–11** can thus be explained by a combination of film morphology and crystal packing effects; for compound **10**, which exhibits exclusively1-D stacking interactions leading to 3-D film growth, poor substrate coverage by the needle-like crystallites led to very low extracted mobilities. In contrast, molecules such as **9** which possess electronic interactions in two dimensions led to two-dimensional film growth, yielding devices with excellent thin-film hole mobility [12]. Two-dimensional film growth alone is not sufficient for good OFET performance: derivative **11** adopts a 2-D π-stacked motif in the solid-state, and does undergo two-dimensional thin-film growth—however, the large separation between π-faces in the crystal (3.8 Å) leads to poor intermolecular electronic coupling and thus low hole mobility in transistor devices.

4. Conclusion

Studies of a homologous series of alkyl-substituted functionalized ADTs (**9–11**) revealed a strong relationship between interactions in the single-crystal, the morphology of the solution-cast films and the performance of the resulting transistor devices. Only in derivatives exhibiting close intermolecular contacts in two dimensions both the film morphology and the intermolecular electronic coupling were sufficient for the formation of high-performance OTFTs, in this case yielding hole mobility of 0.1–0.4 cm^2 V^{-1} s^{-1} for derivative **9**. Where crystal packing yielded strong intermolecular coupling with 3-D film growth, or weak intermolecular coupling with 2-D film growth, device performance was decreased by several orders of magnitude. These results emphasize the need for precise control over semiconductor crystal packing, as the difference between a high-performance and low-performance material arose from shifts of as little as 0.3 Å in inter-stack spacing. The quantification of such structural parameters suggests the potential to screen potential OFET targets by single-crystal X-ray diffraction analysis, which will speed up the development of new materials.

Acknowledgements

References

1 M. J. Deen, M. H. Kazemeini, Y. M. Haddara, J. Yu, G. Vamvounis, S. Holdcroft and W. Woods, *IEEE Trans. Electron Devices*, 2004, **51**, 1892.

2 Y. Wu, Y. Li, B. Ong, P. Liu, S. Gardner and B. Chiang, *Adv. Mater.*, 2005, **17**, 185.

3 M. Mizukami, N. Hirohata, T. Iseki, K. Ohtawara, T. Tada, S. Yagyu, T. Abe, T. Suzuki, Y. Fujisaki, Y. Inoue, S. Tokito and T. Kurita, *IEEE Electron Device Lett.*, 2006, **27**, 249.

4 C. D. Sheraw, T. N. Jackson, D. L. Eaton and J. E. Anthony, *Adv. Mater.*, 2003, **15**, 2009.

5 M. M. Payne, S. R. Parkin, J. E. Anthony, C. C. Kuo and T. N. Jackson, *J. Am. Chem. Soc.*, 2005, **127**, 4986.

6 A. Troisi, G. Orlandi and J. E. Anthony, *Chem. Mater.*, 2005, **17**, 5024.

7 O. Ostroverkhova, D. G. Cooke, F. A. Hegmann, R. R. Tykwinski, S. R. Parkin and J. E. Anthony, *Appl. Phys. Lett.*, 2006, **89**, 192113.

8 H. Sirringhaus, N. Tessler and R. H. Friend, *Science*, 1998, **280**, 1741; H. Sirringhaus, N. Tessler and R. H. Friend, *Synth. Met.*, 1999, **102**, 857.

9 M. Halik, H. Klauk, U. Zschieschang, G. Schmid, S. Ponomarenko, S. Kirchmeyer and W. Weber, *Adv. Mater*, 2003, **15**, 917.

10 M. L. Tang, A. D. Reichardt, T. Siegrist, S. C. B. Mannsfeld and Z. Bao, *Chem. Mater.*, 2008, **20**, 4669.

11 J. G. Laquindanum, H. E. Katz and A. J. Lovinger, *J. Am. Chem. Soc.*, 1998, **120**, 664.

12 Z. Otwinowski and W. Minor, Macromolecular Crystallography Part A, in *Methods in Enzymology*, ed. C. W. Carter and R. M. Swet, Academic Press, London, 1997, vol. 276, pp. 307–326..

13 G. M. Sheldrick, *Acta Crystallogr., Sect. A: Fundam. Crystallogr.*, 2008, **64**, 112.

14 M. Bendikov, F. Wudl and D. F. Perepichka, *Chem. Rev.*, 2004, **104**, 4891.

15 J. E. Anthony, D. L. Eaton and S. R. Parkin, *Org. Lett.*, 2001, **4**, 15.

16 J. Anthony, *Chem. Rev.*, 2006, **106**, 5028.

17 H. Klauk, M. Halik, U. Zschieschang, G. Schmid, W. Radllik and W. Weber, *J. Appl. Phys.*, 2002, **92**, 5259.

18 V. Podzorov, S. E. Sysoev, E. Loginova, V. M. Pudalov and M. E. Gershenson, *Appl. Phys. Lett.*, 2003, **83**, 3504; V. Podzorov, E. Menard, A. Borissov, V. Kiryukhin, J. A. Rogers and M. E. Gershenson, *Phys. Rev. Lett.*, 2004, **93**, 086602.

19 S. Seo, B.-N. Park and P. G. Evans, *Appl. Phys. Lett.*, 2006, **88**, 232114.

20 F. Cicoira, J. A. Miwa, D. F. Perepichka and F. Rosei, *J. Phys. Chem. A*, 2007, **111**, 12674.

21 P. Kastler, W. Pisula, D. Wasserfallen, T. Pakula and K. Müllen, *J. Am. Chem. Soc.*, 2005, **127**, 4286. For a recent detailed review, see: S. Sergeyev, W. Pisula and Y. H. Geerts, *Chem. Soc. Rev.*, 2007, **36**, 1902.

22 P. De la Cruz, N. Martin, F. Miguel, C. Seoane, A. Albert, H. Cano, A. Gonzalez and J. M. Pingarron, *J. Org. Chem.*, 1992, **57**, 6192.

23 M. M. Payne, S. A. Odom, S. R. Parkin and J. E. Anthony, *Org. Lett.*, 2004, **6**, 3325.

24 R. Schmidt, S. Göttling, D. Leusser, D. Stalke, A.-M. Krause and F. Würthner, *J. Mater. Chem.*, 2006, **16**, 3708.

25 O. Kwon, V. Coropceanu, N. E. Gruhn, J. C. Durivage, J. G. Laquindanum, H. E. Katz, J. Cornil and J. L. Bredas, *J. Chem. Phys.*, 2004, **120**, 8186.

26 C. C. Kuo, M. M. Payne, J. E. Anthony and T. N. Jackson, *Tech. Dig. – Int. Electron. Dev. Meet.*, 2004, 373.

27 K. C. Dickey, J. E. Anthony and Y.-L. Loo, *Adv. Mater.*, 2006, **18**, 1721.

28 W. H. Lee, D. H. Kim, J. H. Cho, Y. Jang, J. A. Lim, D. Kwak and K. Cho, *Appl. Phys. Lett.*, 2007, **91**, 092105.

29 M. T. Lloyd, A. C. Mayer, S. Subramanian, D. A. Mourey, D. J. Herman, A. V. Bapat, J. E. Anthony and G. G. Malliaras, *J. Am. Chem. Soc.*, 2007, **129**, 9144.

30 K. C. Dickey, S. Subramanian, J. Anthony, L.-H. Han, S. Chen and Y.-L. Loo, *Appl. Phys. Lett.*, 2007, **90**, 244103.

This journal is © The Royal Society of Chemistry 2009

J. Mater. Chem., 2009, **19**, 7984–7989 | 7989